Materials Research Bulletin 45 (2010) 165–173

Contents lists available at ScienceDirect

Materials Research Bulletin

journal homepage: www.elsevier.com/locate/matresbu

Preparation of size-controlled tungsten oxide nanoparticles and evaluation of their adsorption performance

Darmawan Hidayat [a], Agus Purwanto [b], Wei-Ning Wang [c], Kikuo Okuyama [a,*]

[a] Department of Chemical Engineering, Graduate School of Engineering, Hiroshima University, Higashi-Hiroshima 739-8527, Japan
[b] Department of Chemical Engineering, Faculty of Engineering, Sebelas Maret University, Jl. Ir. Sutami 36 A, Surakarta, Central Java 57126, Indonesia
[c] Department of Energy, Environmental and Chemical Engineering, School of Engineering and Applied Science, Washington University in St. Louis, St. Louis, MO 63130, USA

ARTICLE INFO

Article history:
Received 12 May 2009
Received in revised form 7 August 2009
Accepted 22 September 2009
Available online 27 September 2009

Keywords:
A. Oxide
A. Semiconductors
C. Electron microscopy
D. Surface properties

ABSTRACT

The present study investigated the effects of particle size on the adsorption performance of tungsten oxide nanoparticles. Nanoparticles 18–73 nm in diameter were prepared by evaporation of bulk tungsten oxide particles using a flame spray process. Annealing plasma-made tungsten oxide nanoparticles produced particles with diameters of 7–19 nm. The mechanism of nanoparticle formation for each synthetic route was examined. The low-cost, solid-fed flame process readily produced highly crystalline tungsten oxide nanoparticles with controllable size and a remarkably high adsorption capability. These nanoparticles are comparable to those prepared using the more expensive plasma process.

1. Introduction

Tungsten oxide (WO_3) is an n-type semiconductor metal oxide with an optical band gap of approximately 2.5 eV, and thus is light-activated by irradiation with visible light at a wavelength of approximately 500 nm [1]. Due to its distinctive photocatalytic, electrochromic, and photochromic properties, tungsten oxide is widely used in environmentally friendly and energy-renewal applications, such as solar-powered water splitting, smart-windows, gas-sensing, and dye photodegradation [2–5]. Optimal performance of these technologies is dependent on tungsten oxide surface adsorption.

A better understanding of surface adsorption on nanosized tungsten oxide particles might lead to improved applications, especially in the fields of gas-sensing and catalyst activity. Compared with the bulk form, tungsten oxide nanoparticles exhibit considerably enhanced properties. For example, electrochromic performance is enhanced by reduction of particle size, which allows for fast metal-ion-insertion kinetics. In addition, the greater surface area of nanosized tungsten oxide allows for greater adsorption and light harvesting, which might enhance photocatalytic performance. Meanwhile, highly crystalline tungsten oxide nanoparticles are valuable because amorphous tungsten oxide suffers from high dissolution in acidic solutions, which limits its use in applications despite superior photochromic properties [6,7]. Moreover, controlling the size of tungsten oxide nanoparticles enhances visible light photodegradation, which is suitable for indoor photodegradation or when ultraviolet radiation is unavailable [8,9]. For this reason, efficient methods that allow preparation of size-controlled tungsten oxide nanoparticles are desirable.

Currently, several methods are available for the preparation of tungsten oxide nanoparticles: combustion synthesis, thermal evaporation, hydrothermal processes, and sol–gel [10–12]. However, these methods do not offer the advantage of controllable size, which is required for investigation of the size-dependence of tungsten oxide nanoparticle adsorption performance. In addition, these processes are energy-intensive and time-consuming, which limit their use in industrial applications.

A potential alternative method for the synthesis of nanoparticles with controllable size, morphology and crystallinity is the flame spray technique. Using this process, our group has successfully prepared nanoparticles with enhanced properties from various materials, including yttrium aluminum garnet, barium titanate, and yttria synthesized from liquid precursors [13–15]. In addition, we also prepared non-crystalline silica nanoparticles via solid evaporation, which is also known as solid-fed flame synthesis [16]. In this route, bulk materials, such as micron- or submicron-sized particles, are used as the nanoparticle precursor, which offers tremendous advantages, such as reduced material and process costs, short-processing time, and continuous operation.

* Corresponding author. Tel.: +81 824 24 7716; fax: +81 824 24 7850.
E-mail address: okuyama@hiroshima-u.ac.jp (K. Okuyama).

0025-5408/$ – see front matter © 2009 Elsevier Ltd. All rights reserved.
doi:10.1016/j.materresbull.2009.09.025

Hence, the primary purpose of the present study was to prepare crystalline tungsten oxide nanoparticles of various sizes via a solid-fed flame process to investigate the size-dependence of adsorption. Nanoparticle size and crystallinity were controlled by manipulation of either the carrier- or the fuel-gas flow rate. In addition, commercially available tungsten oxide nanoparticles that were produced using a plasma process were used as the raw material. The commercially available nanoparticles were annealed in a furnace at various temperatures for the preparation of nanoparticles less than 20 nm in diameter. The effects of particle size on adsorption performance were evaluated.

2. Experimental

2.1. Preparation of nanoparticles with controlled sizes

The experimental setup used for the flame process, depicted in Fig. 1, has been described in detail elsewhere [16]. In the present study, we used methane flow rates in the range of 0.5–2.0 L/min with an oxygen–methane volume ratio of 2.5 to ensure complete combustion in the flame. Oxygen was used as the carrier gas and the flow rate was varied between 2 and 10 L/min. A commercially available tungsten oxide powder with a mean particle size, d_p, of 716 nm and a deviation, σ_p, of 1.5 (Nittan Co., Japan) was used as the precursor—yellow in color, non-spherical in morphology and used with no additional treatment. The powder was fed into the flame reactor using an RGB-1000 solid particle disperser (Palas GmbH., Germany) to produce size-controlled nanoparticles via the solid evaporation route [16]. The plasma-synthesized precursor was annealed using a furnace (KDF 1700, Denko, Japan). Tungsten oxide nanoparticles with a diameter of 7 nm (σ_p of 1.3), synthesized using the plasma method, were annealed at various

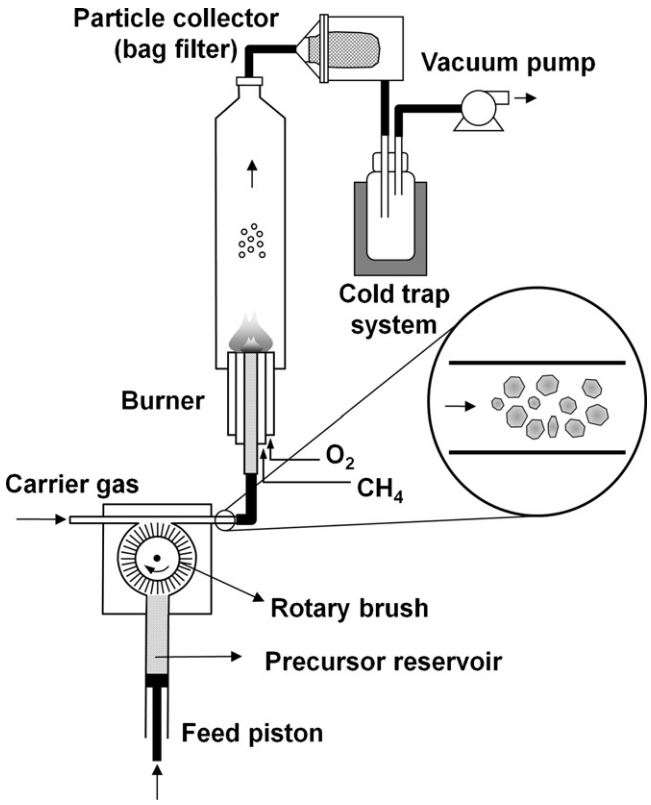

Fig. 1. Experimental setup for the preparation of tungsten oxide nanoparticles via a flame-based, solid evaporation route.

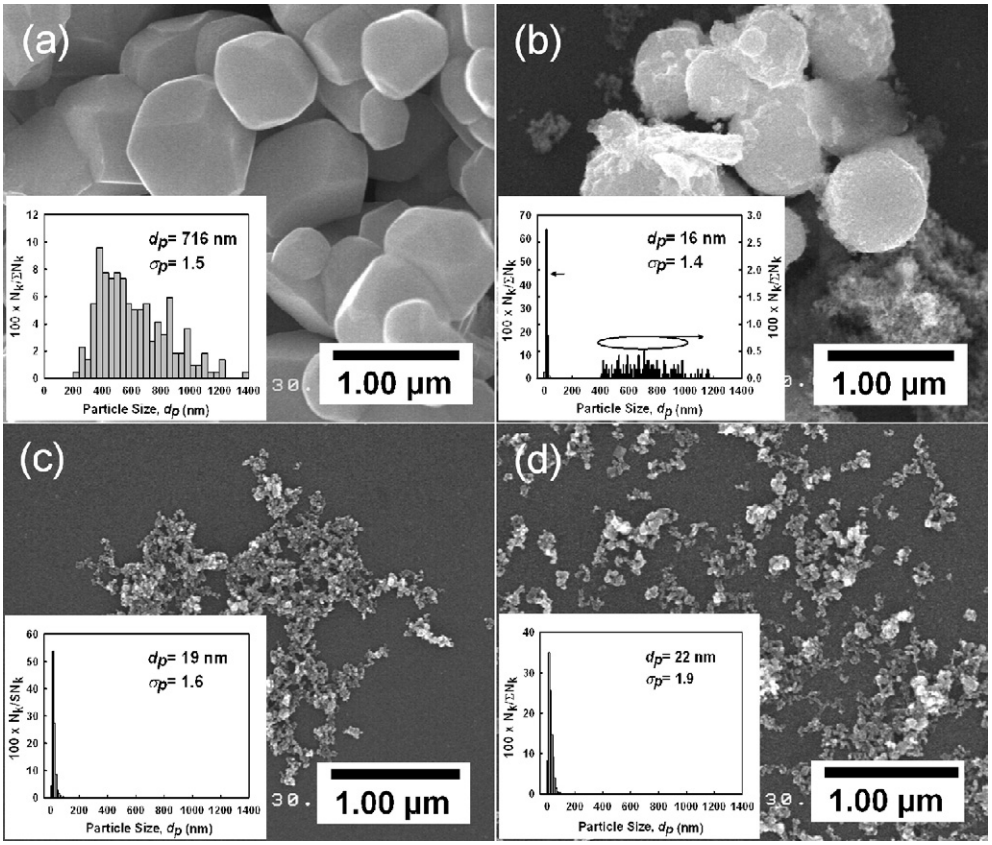

Fig. 2. FE-SEM images of tungsten oxide nanoparticles (a) initial precursor with a size of 716 nm. Tungsten oxide nanoparticles prepared at carrier gas flow rate of 10 L/min and methane flow rates of (b) 0.5 L/min, (c) 0.8 L/min, or (d) 1.0 L/min.

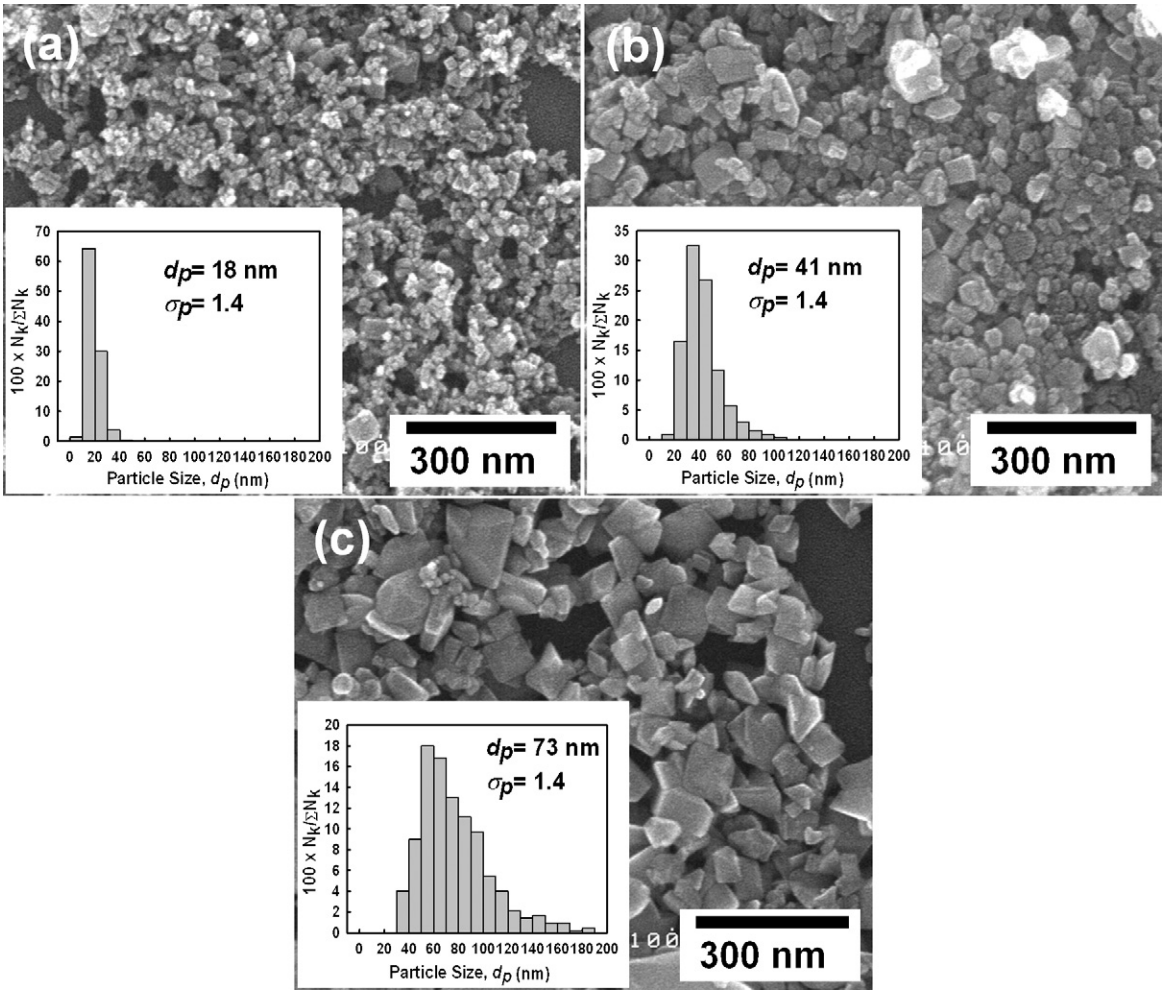

Fig. 3. Size-controlled tungsten oxide nanoparticles prepared using different methane and carrier gas flow rates of (a) 0.7 and 6 L/min, (b) 1.0 and 2 L/min and (c) 2.0 and 10 L/min, respectively.

temperatures to prepare size-controlled tungsten oxide nanoparticles. During each annealing process, one gram of tungsten oxide was annealed. The furnace temperature was increased at the rate of 10 °C/min starting at room temperature. The particles were annealed at predetermined temperatures and allowed to cool to room temperature. The following annealing temperatures were used: 300, 400, 500, 600, and 800 °C. Tungsten oxide nanoparticles of various sizes, all less than 100 nm in diameter were produced.

2.2. Characterization of nanoparticles

The morphology and size of the resulting particles were determined using a field emission scanning electron microscope (FE-SEM, S-5000, Hitachi Corp., Tokyo, Japan) operated at 20 kV.

Table 1
Mean and standard deviation of particle size prepared at various methane and carrier gas flow rates.

Sample	Gas flow rate (L/min)		GMD, d_p (nm)	GSD, σ_p (nm)	Size distribution
	Methane	Carrier gas			
Fig. 2b	0.5	10	16	1.4	Bimodal
Fig. 2c	0.8	10	19	1.6	Monodisperse
Fig. 2d	1	10	22	1.9	Monodisperse
Fig. 3c	2	10	73	1.4	Monodisperse
Fig. 3a	0.7	6	18	1.4	Monodisperse
Fig. 3b	1	2	41	1.4	Monodisperse

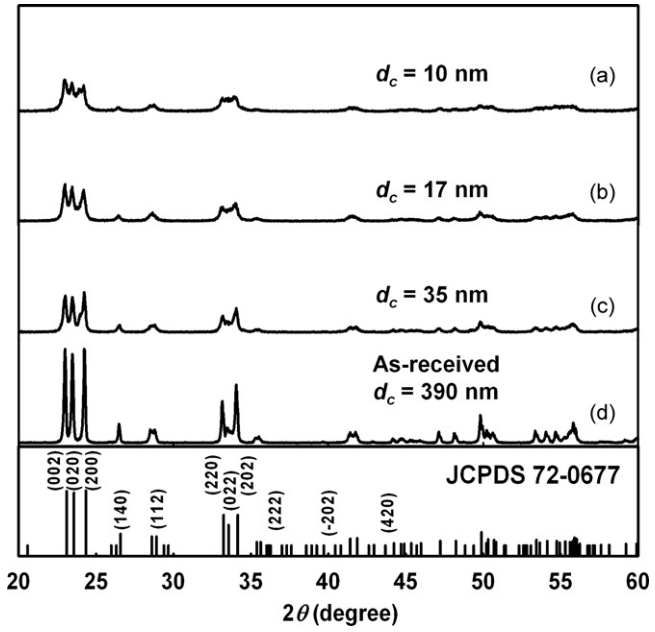

Fig. 4. XRD patterns of tungsten oxide nanoparticles prepared using the flame method and methane and carrier gas flow rates of (a) 0.7 and 6 L/min, (b) 1.0 and 2 L/min, (c) 2.0 and 10 L/min, respectively; and (d) submicron precursor (as-received).

Table 2
Lattice parameters and characteristic peaks of prepared tungsten oxide nanoparticles.

Sample	Gas flow rate (L/min)		Lattice parameters				Characteristic peaks		
	Methane	Carrier gas	a (Å)	b (Å)	c (Å)	β (°)	d_{002} (Å)	d_{020} (Å)	d_{200} (Å)
JCPDS 72-0677	–	–	7.306	7.540	7.692	90.88	3.846	3.770	3.653
Fig. 4a	0.7	6	7.340	7.527	7.678	90.72	3.867	3.792	3.675
Fig. 4b	1	2	7.326	7.535	7.690	90.69	3.857	3.786	3.672
Fig. 4c	2	10	7.312	7.534	7.691	90.75	3.860	3.786	3.669
Fig. 4d	As-received		7.302	7.536	7.692	90.67	3.857	3.780	3.660

The mean and standard deviation of the prepared-particle size were expressed as the geometric mean diameter (GMD, d_p) and the geometric standard deviation (GSD, σ_p), respectively. They were calculated using the equations $\log d_p = \sum n \log d / \sum n$, and $\log \sigma_p = \{\sum[n(\log d - \log d_p)^2]/\sum n\}^{1/2}$, respectively, and the corresponding FE-SEM images of approximately 1000 randomly sampled particles used d as the size of particle size of samples [17]. Crystallinity was analyzed using powder X-ray diffraction (XRD, RINT 2200V, Rigaku Denki, Tokyo, Japan) with nickel-filtered Cu Kα radiation (wavelength, λ = 1.504 Å), an operating voltage of 40 kV, a scan step of 0.02°, and a scan speed of 4 °/min. The MAUD (Material Analysis Using Diffraction) program was used for Rietveld refinement of the XRD patterns for phase identification of the prepared particles. The crystal structure of the prepared particles was analyzed using a field emission transmission electron microscope (FE-TEM; JEM-3000F, JEOL, Tokyo, Japan) operated at 300 kV. Furthermore, crystallinity was also analyzed using selected area electron diffraction (SAED). Chemical composition was determined using scanning transmission electron microscopy (STEM) coupled with energy dispersive X-ray spectroscopy (EDS).

2.3. Evaluation of adsorption performance

Methylene blue (MB), $C_{16}H_{18}C_lN_3S$, was employed to probe the adsorption performance of the prepared tungsten oxide nanoparticles. An aqueous solution (250 mL) of methylene blue (4.5 mg/L) and tungsten oxide (200 mg/L) was loaded into a sealed, dark glass tube, which served as the test-reactor. To prevent temperature-induced changes in the methylene blue concentration, the temperature of the reactor was maintained at 5 °C by circulating cold water through the outer tubular container. During the 30-min adsorption test, the solution was continuously aerated with dry air at a flow rate of 100 cm^3/min. Changes in the methylene blue concentration were measured using a UV–vis spectrophotometer (Shimadzu 2540, Japan). Prior to each concentration measurement, an aliquot of the suspension was centrifuged at 15,000 rpm for 5 min using a high-speed centrifuge (Himac, CR 21G, Hitachi, Japan) to separate tungsten oxide adsorbing methylene blue from the suspension. Adsorption performance was evaluated by measuring the methylene blue concentration of the suspension every 5–10 min.

3. Results and discussion

In a flame process, the methane flow rate determines the flame temperature, which, in turn, significantly affects the morphology, size distribution and crystallinity of the prepared particles [13]. Fig. 2 shows the size variation of the as-received and prepared particles at a fixed carrier gas flow rate of 10 L/min and at varied methane flow rates of 0.5, 0.8 and 1.0 L/min. The as-received particles were non-spherical with a size of 716 nm (σ_p of 1.5), as shown in Fig. 2a. When the methane flow rate was 0.5 L/min (Fig. 2b), particle size decreased slightly and tungsten oxide vapor condensed on the particle surface. In addition, 16-nm nanoparticles (σ_p of 1.4) were produced via evaporation, resulting in a bimodal size distribution (inset of Fig. 2b). This result is indicative of partial evaporation of the particles due to an insufficient flame temperature. Subsequently, when the methane flow rate was increased to 0.8 or 1.0 L/min, the particles evaporated completely, generating nanoparticles (Fig. 2c and d). This result was evident in the disappearance of submicron particles and the formation of nanoparticles, the size distributions of which are shown in the figure insets. A methane flow rate of 0.8 or 1.0 L/min produced similarly sized particles—19 nm (σ_p of 1.6) and 22 nm (σ_p of 1.9), respectively, as shown in the insets of Fig. 2c and d. Thus, particle size was significantly reduced compared with the as-received particles. In addition, the prepared nanoparticles were non-spherical and non-agglomerated.

Methane flow rates of 0.5–2.0 L/min produce flame temperatures of approximately 700–1300 °C, which are lower than the

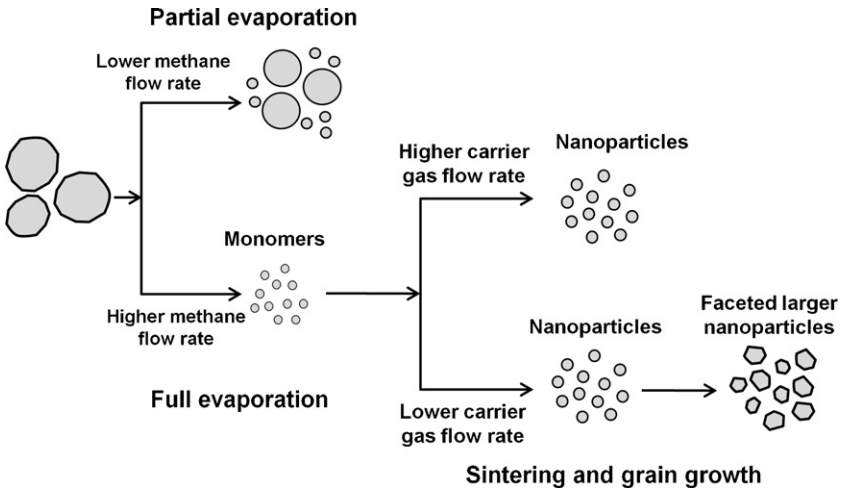

Fig. 5. Proposed mechanism by which tungsten oxide nanoparticles prepared via a flame-based, solid evaporation route form.

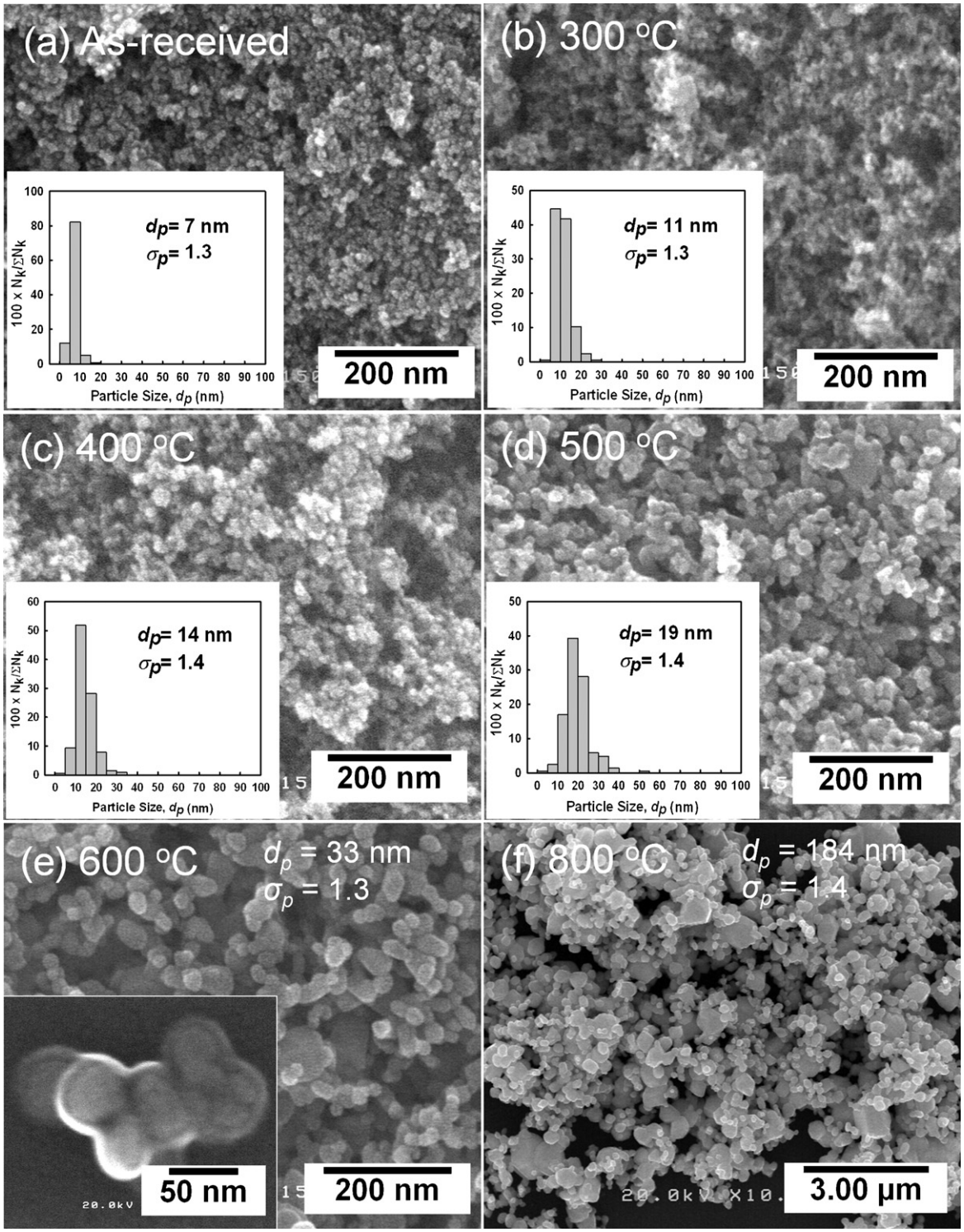

Fig. 6. Size-controlled tungsten oxide nanoparticles derived from nanoparticles synthesized using a plasma method by variation of annealing temperature: (a) as-received, (b) 300 °C, (c) 400 °C, (d) 500 °C, (e) 600 °C or (f) 800 °C after 30 min of annealing.

melting point of bulk tungsten oxide (1473 °C). Therefore, vapor pressure, rather than melting point, is the key factor in evaporation of solid tungsten oxide. The flame temperature used in the present study produced vapor pressure sufficient to evaporate the tungsten oxide. Similar approaches have been used for the evaporation of various volatile metal oxides [16,18]. The formation of tungsten oxide nanoparticles is thought to occur via gas-to-particle conversion, during which vapor nucleation, condensation, and coagulation take place. At a methane flow rate of 0.5 L/min, the temperature was too low for full evaporation of tungsten oxide particles. Due to heat inadequacy, evaporation occurred only on the particle surface, resulting in slightly smaller particles, as shown in Fig. 2b. Therefore, in addition to nanoparticles, partially evaporated particles, which disappeared as the methane flow rate increased, were produced. This result is consistent with our previous report on the preparation of silica nanoparticles [16]. Vapor pressure increased with flame temperature, which was elevated by increasing the methane flow rate. Thus, the size

distribution of the prepared tungsten oxide nanoparticles could be controlled by adjusting the evaporation rate via changes in the methane flow rate.

In general, the properties of metal oxide nanoparticles are size-dependent. When prepared in nanosized particles, metal oxides exhibit unique chemical and physical properties, catalytic activity in particular, that are remarkably different from those of the corresponding bulk materials. Therefore, control of particle size by manipulation of either the methane or carrier gas flow rate was investigated (Fig. 3). Particles with a diameter of 18 nm (σ_p of 1.4) were produced using a methane flow rate of 0.7 L/min and a carrier gas flow rate of 6 L/min, as shown in Fig. 3a. Comparison of Figs. 2d and 3b reveals the effect of reducing the carrier gas flow rate from 10 to 2 L/min. At a constant methane flow rate of 1.0 L/min, particle size, d_p, increased to 41 nm (σ_p of 1.4) with a reduction in the carrier gas flow rate. Conversely, increasing the methane flow rate to 2.0 L/min at a carrier gas flow rate of 10 L/min, increased d_p to 73 nm (σ_p of 1.4), as shown in Fig. 3c. These results indicate that particle size can be controlled by manipulation of either the methane or the carrier gas flow rates. As the carrier gas flow rate was reduced, the residence time was increased, resulting in the formation of larger particles due to increased cluster growth on the surface of the tungsten oxide nanoparticles. By contrast, as the methane flow rate was increased to 2.0 L/min, larger particles formed due to sintering of nanoparticles in the flame reactor. Table 1 summarizes the methane and carrier gas flow rate settings and the corresponding sizes and deviations. These values show that control of size distribution from bimodal to monodisperse distribution can be carried out by controlling either the methane or the carrier gas flow rates.

A longer residence time due to reduced carrier gas flow allowed a longer crystallization period. Nogueira et al. found that both particle shape and size are altered by longer crystallization periods [19]. Because crystal structure is closely related to the properties of the particles [20], it is important to investigate their crystallinity. Fig. 4 shows the XRD patterns of the tungsten oxide nanoparticles prepared using the flame process and the conditions shown in Fig. 3. The XRD patterns of the as-received submicron particles are also shown (Fig. 4d). The diffraction peaks of the XRD patterns shown in Fig. 4 suggest that the prepared tungsten oxide nanoparticles were highly crystallized. In addition, Table 2 compares the refined lattice parameters of prepared particles along with their three characteristic peaks of monoclinic tungsten oxide. As shown, the lattice parameters of crystal structures are in accordance with those in JCPDS 72-0677. Moreover, the lattice spaces of three distinct characteristic XRD peaks corresponding to (0 0 2), (0 2 0) and (2 0 0) plane orientations at 2θ positions of 23.11°, 23.58° and 24.35°, respectively, were also found to follow those of JCPDS 72-0677. Hence, these results strongly indicated the formation of a monoclinic crystal structure of prepared tungsten oxide nanoparticles in the space group ($P21/n$).

Crystallite sizes, determined using Scherrer's formula, were 10, 17 and 35 nm for particles prepared using methane flow rates of 0.7, 1.0 and 2.0 L/min, respectively. Crystallite size decreased with decreasing particle size, as indicated by the broadening of the measured XRD peaks. At smaller particle sizes, lattice fringe (0 0 2) was predominant, while larger particles showed a (2 0 0) orientation. The altered lattice orientation also confirms the change in shape evident in Fig. 3c, which shows faceted particles. This result strongly suggests that the decrease in crystallite size was verified by the formation of smaller crystalline tungsten oxide nanoparticles. The TEM images shown in Fig. 8 provide support for the formation of crystalline tungsten oxide.

The proposed mechanism by which tungsten oxide forms via solid evaporation during the flame process is illustrated in Fig. 5. We suggest that both solid evaporation and sintering of nanoparticles are involved in the formation of tungsten oxide nanoparticles. Initially, the evaporation of solid tungsten oxide was determined by flame temperature, which was controlled by the methane flow rate. Partial evaporation was observed at inadequate methane flow rates. By contrast, high methane flow rates resulted in complete evaporation of the solid tungsten oxide and in the production of nanoparticles. In addition to the methane flow rate, the carrier gas flow rate determined the residence time and, consequently, controlled the grain growth of monomers originating from evaporation. Longer residence times result from reduced carrier gas flow rates. Thus, larger nanoparticles result from both sintering and increased grain growth.

We found that use of a methane flow rate of 0.7 L/min reduced particle size to 18 nm. However, methane flow rates of less than 0.7 L/min resulted in larger particles due to partial evaporation. To produce particles less than 20 nm in diameter, an annealing route was applied using 7-nm nanoparticles, produced via a plasma method, as precursors. Annealing in a furnace for 30 min at 300, 400 and 500 °C produced particles 11, 14 and 19 nm in diameter, respectively. Particle size was uniformly distributed and increased with annealing temperature, as shown in Fig. 6. Hence, a set of tungsten oxide nanoparticles with a size range of 7, 11, 14 and 19 nm were produced via sintering for subsequent investigation of adsorption activity. Particle enlargement was initiated by sintering of several nanoparticles, which was caused by a reduction in the total interfacial energy of the particles, as shown in the inset of Fig. 6e. Use of higher annealing temperatures, i.e., 600 or 800 °C, produced larger particles, resulting in grain coarsening, as shown in Fig. 6e and f. The XRD results shown in Fig. 7 show that the crystallite size of sintered tungsten oxide increased with annealing temperature. Thus, the increase in crystallite size confirmed that nanoparticle sintering resulted in larger particles.

The details of crystallinity for the (as-received, plasma-made; 500 °C annealed; and, flame-made) tungsten oxide nanoparticles are represented by their TEM images, as shown in Fig. 8. All particles were uniform, non-agglomerated, and highly crystallized, and crystallite size was consistent with that calculated from the corresponding XRD patterns. Moreover, the SAED patterns showed many diffraction rings, indicating polycrystalline particles

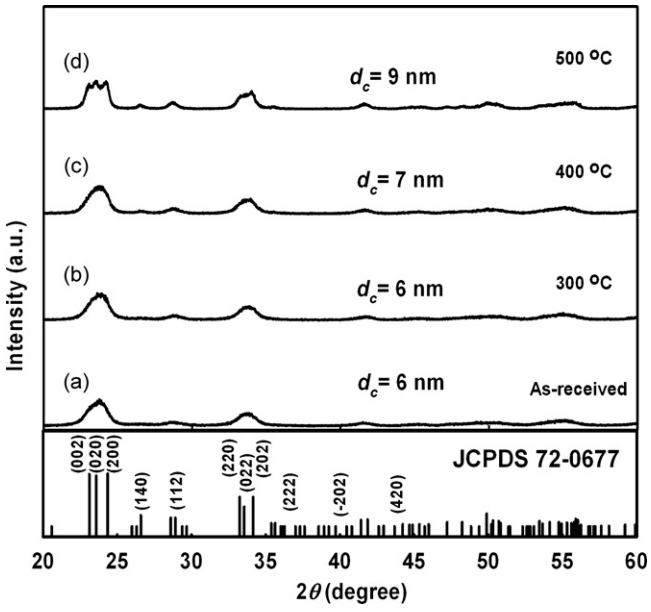

Fig. 7. XRD patterns of (a) nanoparticles synthesized using a plasma method (initial precursor) and sintered tungsten oxide nanoparticles prepared by annealing for 30 min at various annealing temperatures of (b) 300 °C, (c) 400 °C or (d) 500 °C.

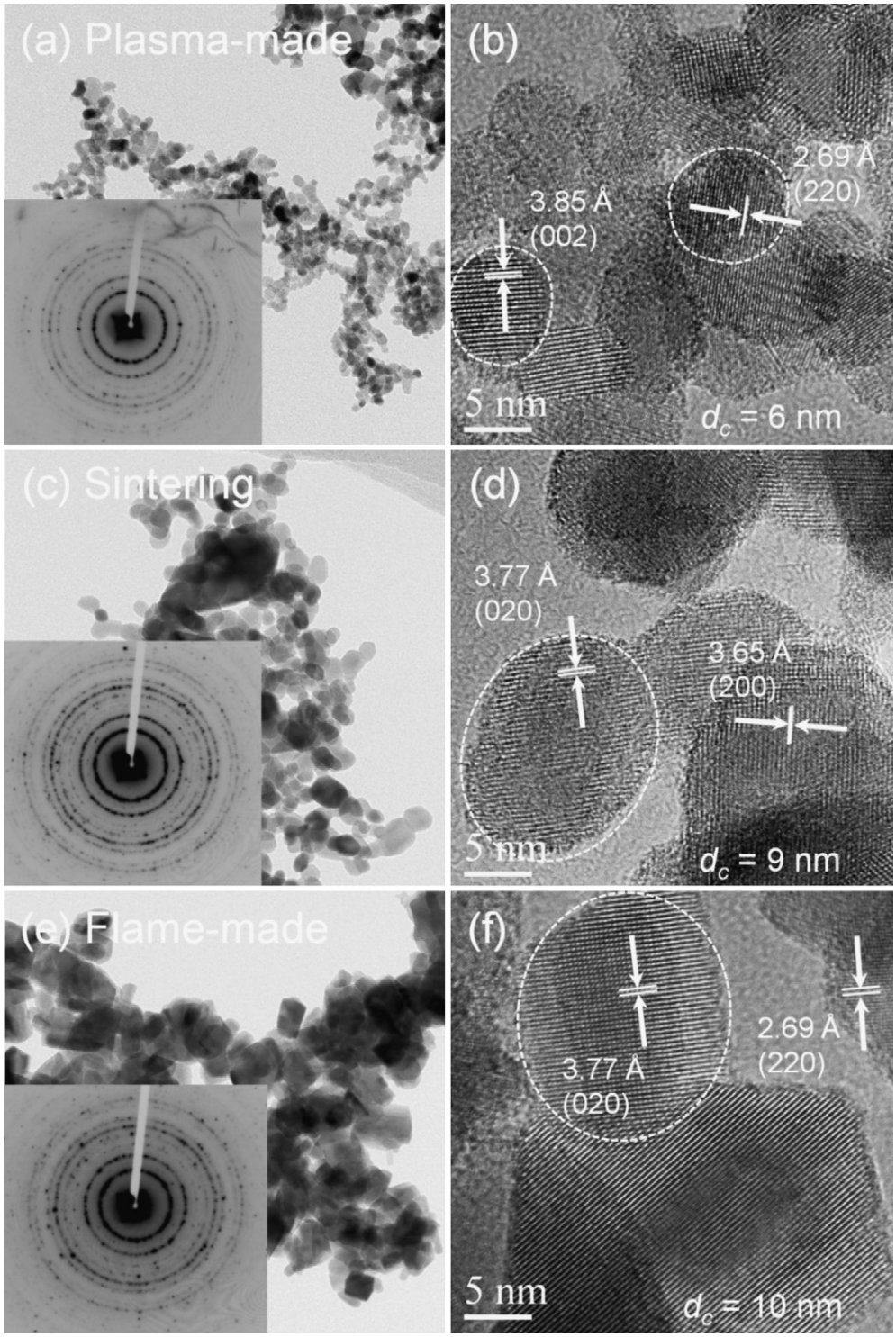

Fig. 8. TEM, HR-TEM and SAED images, respectively, of prepared tungsten oxide nanoparticles: (a) and (b) as-received, (c) and (d) sintered at 400 °C and (e) and (f) synthesized using the flame method.

comprised of crystals with various lattice orientations. HR-TEM verified the polycrystallinity of the prepared particles (Fig. 8b, d and f). These highly ordered lattice fringes, even in the surface region, provide evidence that the crystallinity of the particles was well-established. Analysis of the elemental composition of the prepared particles, determined from the EDS spectra (Fig. 9), indicated the formation of a tungsten oxide compound. As no other chemical elements were detected, this result indicated that the prepared tungsten oxide nanoparticles were free of impurities.

Fig. 10 shows the methylene blue adsorption of the prepared tungsten oxide nanoparticles. Within the first 5 min, the methylene blue concentration in the solution decreased significantly, indicating rapid adsorption (Fig. 10a). After 5 min, the adsorption reached equilibrium, as indicated by the relatively constant methylene blue concentration in the suspension. The adsorption performance of prepared tungsten oxide nanoparticles improved with a reduction in particle size, irrespective of the type of precursor used. Based on this result, it was concluded that the

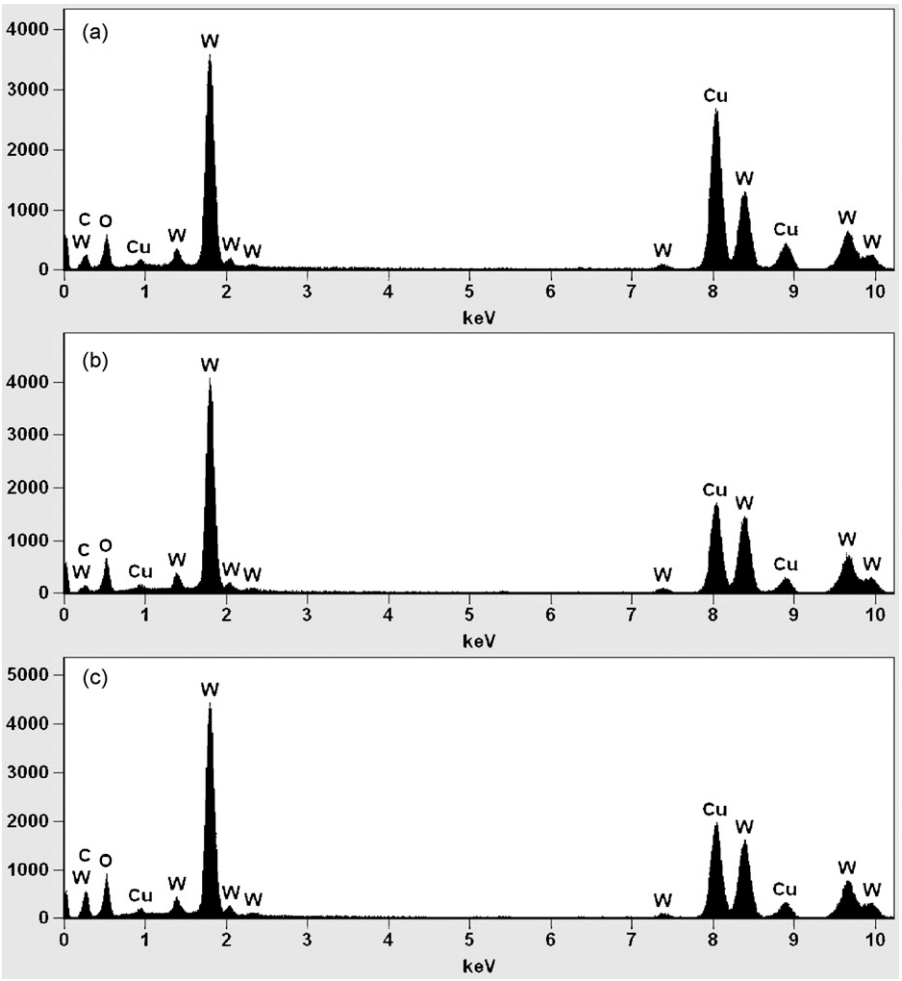

Fig. 9. EDS patterns of prepared tungsten oxide particles (a) synthesized using a plasma method, (b) annealed at 500 °C and (c) synthesized using the flame method.

adsorption performance of tungsten oxide particles is size-dependent. This result is consistent with that reported previously by Morales et al. [21]. Dangling bonds on the surface of metal oxides are a key determinant of adsorption on semiconductor surfaces, thereby governing surface chemistry behavior [22]. Moreover, dangling bonds can be used to identify both nanoparticle structures and properties. In this case, tungsten atoms of the tungsten oxide semiconductor may act as the center of dangling bonds, creating oxygen vacancies on the surface. Previously, surface oxygen vacancies were found to enhance charge transfer from the surface to the adsorbate [23], which increased the interactions between them. Dangling bonds of tungsten oxides on the surface preferentially bind adsorbate molecules—methylene blue molecules in the present study. They become the active centers of adatom adsorption and interaction, and therefore drive thermodynamic processes and chemical reactions. Monolayer adsorption on the particle surface involves an interaction between only adsorbate molecules and the particle surface (Fig. 10b). As the particle size is reduced, both the total specific surface area and dangling-bond density increase; therefore, performance of surface atoms becomes dominant [24]. The increase in adsorption activity of prepared tungsten oxide shown in Fig. 10a provides evidence that the interaction between surface atoms of tungsten oxide and methylene blue molecules was increased with reduction in tungsten oxide particle size. This result demonstrates that the adsorption performance of tungsten oxide is dependent on particle size.

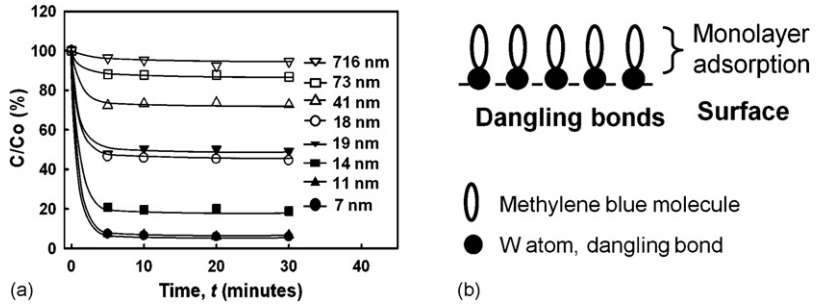

Fig. 10. (a) Adsorption performance of prepared tungsten oxide nanoparticles with various particle sizes and (b) illustration of monolayer adsorption on the surface of tungsten oxide.

4. Conclusion

Size-controlled crystalline tungsten oxide nanoparticles were successfully prepared via a flame-based, solid evaporation route and by the annealing of nanoparticles. For the solid-fed flame process, variation of either the methane or carrier gas flow rate determined the size of the prepared nanoparticles. By contrast, with the annealing route, the temperature determined the particle size. The adsorption of methylene blue by the prepared tungsten oxide nanoparticles was dependent on particle size. The adsorption performance was markedly improved with smaller particles, regardless of the precursor used.

Acknowledgements

The authors thank Mr. Kozo Watanabe for his assistance with this experiment. We are also grateful to Dr. Eishi Tanabe (Hiroshima Prefectural Institute of Industrial Science and Technology) for his help with the TEM characterizations. The Ministry of Education, Culture, Sports, Science and Technology of Japan is acknowledged for providing a doctoral scholarship (D.H.) and a grant-in-aid for scientific research (K.O.).

References

[1] H. Kominami, K. Yabutani, T. Yamamoto, Y. Kera, B. Ohtani, J. Mater. Chem. 11 (2001) 3222–3227.
[2] T. He, J. Yao, J. Mater. Chem. 17 (2007) 4547–4557.
[3] G.A. Niklasson, C.G. Granqvist, J. Mater. Chem. 17 (2007) 127–156.
[4] E. Rossinyol, A. Prim, E. Pellicer, J. Arbiol, F.H. Ramírez, F. Peiró, A. Cornet, J.R. Morante, L.A. Solovyov, B. Tian, T. Bo, D. Zhao, Adv. Funct. Mater. 17 (2007) 1801–1806.
[5] H. Wang, T. Deutsch, J.A. Turner, J. Electrochem. Soc. 155 (2008) F91–F96.
[6] E.L. Miller, B. Marsen, B. Cole, M. Lum, Electrochem. Solid-State Lett. 9 (2006) G248–G250.
[7] S.-H. Lee, R. Deshpande, P.A. Parilla, K.M. Jones, B. To, A.H. Mahan, A.C. Dillon, Adv. Mater. 18 (2006) 763–766.
[8] C. Santato, M. Ulmann, J. Augustynski, Adv. Mater. 13 (2001) 511–514.
[9] Z.-G. Zhao, M. Miyauchi, Angew. Chem. Int. Ed. 47 (2008) 7051–7055.
[10] B. Yan, Y. Xu, N.K. Goh, L.S. Chia, Chem. Commun. (2000) 2169–2170.
[11] B. Yang, P.R.F. Barnes, W. Bertram, V. Luca, J. Mater. Chem. 17 (2007) 2722–2729.
[12] M. Regragui, M. Addou, A. Outzourhit, E.E. Idrissi, A. Kachouane, A. Bougrine, Sol. Energy Mater. Sol. Cells 77 (2003) 341–350.
[13] A. Purwanto, W.-N. Wang, I.W. Lenggoro, K. Okuyama, J. Electrochem. Soc. 154 (2007) J91–J96.
[14] A. Purwanto, W.-N. Wang, I.W. Lenggoro, K. Okuyama, J. Eur. Ceram. Soc. 27 (2007) 4489–4497.
[15] A. Purwanto, I.W. Lenggoro, H. Chang, K. Okuyama, J. Chem. Eng. Jpn. 39 (2006) 68–76.
[16] W. Widiyastuti, A. Purwanto, W.-N. Wang, F. Iskandar, H. Setyawan, K. Okuyama, AIChE J. 55 (2009) 885–895.
[17] W.-N. Wang, W. Widiyastuti, I.W. Lenggoro, T.O. Kim, K. Okuyama, J. Electrochem. Soc. 154 (2007) J121–J128.
[18] Y. Xiong, S.W. Lyons, T.T. Kodas, S.E. Pratsinis, J. Am. Ceram. Soc. 78 (1995) 2490–2496.
[19] H.I.S. Nogueira, A.M.V. Cavaleiro, J. Rocha, T. Trindade, J.D.P. Jesus, Mater. Res. Bull. 39 (2004) 683–693.
[20] Y. Guo, X. Quan, N. Lu, H. Zhao, S. Chen, Environ. Sci. Technol. 41 (2007) 4422–4427.
[21] W. Morales, M. Cason, O. Aina, N.R. de Tacconi, K. Rajeshwar, J. Am. Chem. Soc. 130 (2008) 6318–6319.
[22] F. Ma, K.-W. Xu, Surf. Interface Anal. 39 (2007) 611–614.
[23] M. Epifani, J.D. Prades, E. Comini, E. Pellicer, M. Avella, P. Siciliano, G. Faglia, A. Cirera, R. Scotti, F. Morazzoni, J.R. Morante, J. Phys. Chem. C 112 (2008) 19540–19546.
[24] R.I. Masel, Principles of Adsorption and Reaction on Solid Surfaces, Wiley, New York, 1996.